Snapshot of a Reaction Intermediate: Analysis of Benzoylformate Decarboxylase in Complex with a Benzoylphosphonate Inhibitor†

Gabriel S. Brandt,‡ Malea M. Kneen,§,|| Sumit Chakraborty,⊥ Ahmet T. Baykal,⊥ Natalia Nemeria,⊥ Alejandra Yep,§ David I. Ruby,‡ Gregory A. Petsko,‡ George L. Kenyon,§ Michael J. McLeish,§,|| Frank Jordan,*,⊥ and Dagmar Ringe*,‡

Departments of Chemistry and Biochemistry, Rosenstiel Basic Medical Sciences Research Center, Brandeis University, Waltham, Massachusetts 02454, Department of Chemistry, Rutgers University, Newark, New Jersey 07102, and Department of Medicinal Chemistry, College of Pharmacy, University of Michigan, Ann Arbor, Michigan 48109

Received October 17, 2008; Revised Manuscript Received December 19, 2008

ABSTRACT: Benzoylformate decarboxylase (BFDC) is a thiamin diphosphate- (ThDP-) dependent enzyme acting on aromatic substrates. In addition to its metabolic role in the mandelate pathway, BFDC shows broad substrate specificity coupled with tight stereo control in the carbon−carbon bond-forming reverse reaction, making it a useful biocatalyst for the production of chiral α-hydroxy ketones. The reaction of methyl benzoylphosphonate (MBP), an analogue of the natural substrate benzoylformate, with BFDC results in the formation of a stable analogue (C2α-phosphonomandelyl-ThDP) of the covalent ThDP-substrate adduct C2α-mandelyl-ThDP. Formation of the stable adduct is confirmed both by formation of a circular dichroism band characteristic of the 1′,4′-iminopyrimidine tautomeric form of ThDP (commonly observed when ThDP forms tetrahedral complexes with its substrates) and by high-resolution mass spectrometry of the reaction mixture. In addition, the structure of BFDC with the MBP inhibitor was solved by X-ray crystallography to a spatial resolution of 1.37 Å (PDB ID 3FSJ). The electron density clearly shows formation of a tetrahedral adduct between the C2 atom of ThDP and the carbonyl carbon atom of the MBP. This adduct resembles the intermediate from the penultimate step of the carboligation reaction between benzaldehyde and acetaldehyde. The combination of real-time kinetic information via stopped-flow circular dichroism with steady-state data from equilibrium circular dichroism measurements and X-ray crystallography reveals details of the first step of the reaction catalyzed by BFDC. The MBP-ThDP adduct on BFDC is compared to the recently solved structure of the same adduct on benzaldehyde lyase, another ThDP-dependent enzyme capable of catalyzing aldehyde condensation with high stereospecificity.

Characterizing the discrete steps of a chemical reaction remains an exceptionally difficult task. One strategy for enzyme-catalyzed reactions has been to obtain the structure of the protein catalyst in the presence of a reaction intermediate. In most cases, though, structural determination is relatively slow and the lifetime of relevant intermediates fleeting. The use of molecules that resemble the intermediate but that are longer lasting is an established method for obtaining detailed information on the molecular species formed during an enzyme-catalyzed reaction pathway (*1*−*6*).

Benzoylformate decarboxylase (BFDC,[1] EC 4.1.1.7) catalyzes the decarboxylation of benzoylformate to benzaldehyde (Scheme 1a). A thiamin diphosphate- (ThDP-) dependent enzyme, BFDC plays a fundamental role in mandelate metabolism (*7, 8*). One of several ThDP-dependent enzymes that catalyze the decarboxylation of 2-oxo acids, it has received considerable interest in studies aimed at understanding the substrate specificity in enzymes of this class (*9*−*12*), because of the enzyme's ability to catalyze stereospecific carboligation reactions (*13*−*16*) (Scheme 1b,c).

BFDC was incubated with methyl benzoylphosphonate (MBP, Scheme 2), an analogue of benzoylformate, forming an MBP-ThDP adduct that cannot be decarboxylated (*17*−*21*). The formation of a covalent MBP-ThDP adduct on BFDC was initially followed by time-resolved CD spectroscopy, and its formation was confirmed by mass spectrometry. Finally, the X-ray structure of the MBP-ThDP adduct on BFDC was

† Supported by NIH NRSF F32GM069057 (G.S.B., Brandeis), NIH GM050380 (Rutgers), and NSF EF-0425719 (Brandeis and Michigan).

* To whom correspondence should be addressed. D.R.: e-mail, ringe@brandeis.edu; tel, 781-736-4902; fax, 781-736-2405. F.J.: e-mail, frjordan@newark.rutgers.edu; tel, 973-353-5470; fax, 973-353-1264.

‡ Brandeis University.

§ University of Michigan.

|| Current address: Department of Chemistry and Chemical Biology, IUPUI, Indianapolis, IN 46202.

⊥ Rutgers University.

[1] Abbreviations: BFDC, benzoylformate decarboxylase; ThDP, thiamin diphosphate; MBP, methyl benzoylphosphonate; MAP, methyl acetylphosphate; CD, circular dichroism; BAL, benzaldehyde lyase; MThDP, C2α-mandelylthiamin diphosphate; HBThDP, C2α-hydroxybenzylthiamin diphosphate; IP, 1′,4′-iminopyrimidine tautomer of ThDP; AP, 4′-aminopyrimidine tautomer of ThDP; LThDP, C2α-lactylthiamin diphosphate; POX, pyruvate oxidase; BP, benzoyl phosphonate; 2-HPP, 2-hydroxypropiophenone; ee, enantiomeric excess; Ni-NTA, nickel nitriloacetate resin; PDB, Protein Data Bank; PMThDP, C2α-phosphonomandelyl-ThDP; PLThDP, 1′,4′-iminophosphonolactyl-ThDP; YPDC, yeast pyruvate decarboxylate; TCA, trichloroacetic acid; FTICR, Fourier transform ion cyclotron resonance.

10.1021/bi801950k CCC: $40.75
Published on Web 03/25/2009

Scheme 1: Activity of Benzoylformate Decarboxylase (BFDC) toward Benzoylformate (a), Benzaldehyde (b), and Acetaldehyde with Benzaldehyde (c)

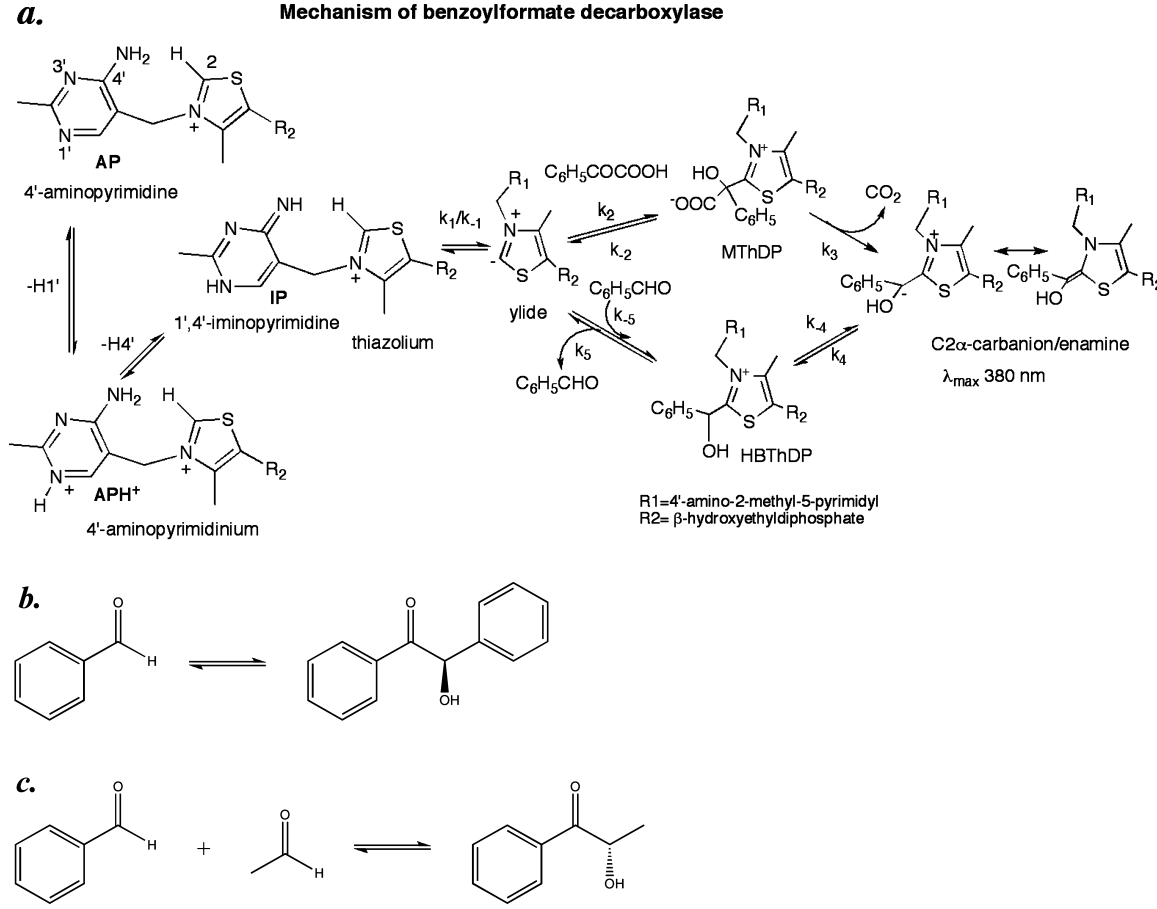

Scheme 2: Mechanism of Formation of the Predecarboxylation Intermediate from Benzoylformate or MBP

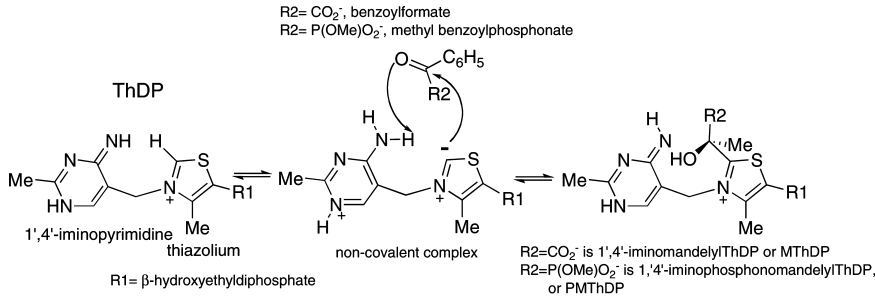

determined and compared with that of the same adduct on benzaldehyde lyase (BAL), a related ThDP-dependent enzyme also acting on aromatic substrates (*22*). BAL has also been investigated for its utility in producing stereospecific 2-hydroxy ketones (*10, 16, 23*−*25*). Although both enzymes form (*R*)-benzoin in >99% ee, BFDC catalyzes formation of 2-(*S*)-hydroxypropiophenone (2-HPP) from benzaldehyde and acetaldehyde in 90% ee. Conversely, BAL produces 2-(*R*)-HPP in 99% ee. The causes of this difference in chiral induction have been the subject of some speculation (*9, 10*). Here we examine, for the first time, structural evidence for the source of the observed stereospecificity on BFDC and BAL.

MATERIALS AND METHODS

Methyl benzoylphosphonate was synthesized as reported elsewhere (*22*). Benzoylformate, NADH, and horse liver alcohol dehydrogenase (HLADH) were purchased from Sigma-Aldrich (St. Louis, MO). All other chemicals purchased were of the highest purity grade available and were used without further purification.

Preparation and Assay of C-Terminally His$_6$-Tagged BFDC. The enzyme was expressed, purified, and stored as described elsewhere (*26*). The activity of BFDC was measured using a NADH/horse liver alcohol dehydrogenase (HLADH) coupled assay (*26*). In a typical assay, 1 mL of the reaction mixture contained in 50 mM KH_2PO_4 (pH 6.0), benzoylformate (3.5 mM), $MgSO_4$ (2.5 mM), ThDP (0.5 mM), NADH (0.28 mM), and 0.25 mg (10 units) of HLADH. The reaction was initiated by the addition of BFDC. The disappearance of NADH was monitored at 340 nm at 30 °C.

The inhibition constant (K_i) for methyl benzoylphosphonate was determined by varying the concentrations of benzoylformate ($0.3-3 \times K_m$) and methyl benzoylphosphonate ($0.3-4 \times K_i$). Initial velocities were then fit to eq 1 using the Enzyme Kinetics package of SigmaPlot 9.0 (Systat Software Inc.).

$$v = \frac{V_{max}[S]}{[S] + K_m\left(1 + \frac{[I]}{K_i}\right)} \quad (1)$$

Circular Dichroism Titration of BFDC by MBP and MAP. To the BFDC (1.7 mg/mL, concentration of active centers = 30.2 μM) in 20 mM KH_2PO_4 (pH 6.0), containing $MgCl_2$ (2.5 mM) and ThDP (0.50 mM) were added aliquots of MBP (0.001−0.50 mM) or MAP (1−30 mM), and CD spectra were recorded in the near-UV region using an Aviv circular dichroism spectrometer (Model 202). Difference spectra were obtained on subtraction of the spectrum of BFDC in the absence of MBP using SigmaPlot 2001 (v.7.101). Values of $K_{d,MBP}$ were calculated by fitting the data to a Hill equation: $CD = (CD_{max}[MBP]^n)/(K_d^n + [MBP]^n)$.

Stopped-Flow CD. Experiments were carried out on a π^*-180 CDF spectrometer from Applied Photophysics. In a typical experiment, BFDC (83 μM active site concentration) in 50 mM KH_2PO_4 (pH 6.0) containing 2.5 mM $MgSO_4$ and 0.5 mM ThDP (buffer A) was mixed with an equal volume of substrate of intended concentration in the same buffer. The reaction was monitored for varied times (0.01−200 s), and data points were collected at varied time intervals (2.5−10 ms). A slit width of 2 mm and a path length of 10 mm were used. The temperature was maintained at 30 °C. The data were analyzed using Pro-K Global Analysis software. SigmaPlot 2001 version 7.101 was used for data analysis.

Protein Crystallization. BFDC was concentrated to 30−40 mg/mL in its storage buffer (100 mM potassium phosphate, pH 6.0, 1 mM $MgSO_4$, 0.5 mM ThDP, 10% glycerol) and could be stored at −80 °C for up to several months prior to crystallization. Under the conditions of Hasson et al. (*27*) for hanging drop vapor diffusion, the protein crystallized from heavy precipitate to give very large, well-formed prisms in a matter of days. A 1 M solution of MBP was utilized at a 1:50 dilution for cocrystallization studies. The MBP was diluted 1:5 into protein storage buffer and then incubated 1:10 with protein solution on ice for 10−15 min. One microliter of this BFDC-MBP solution was mixed with 1 μL of well solution [100 mM Tris-HCl (pH 8.5), 150 mM $CaCl_2$, 0.5% (v/v) MPD, 22% (v/v) PEG 400] and left to stand over the well solution in a hanging drop vapor diffusion tray. As with protein alone, large crystals formed in 3−5 days. After transfer to fresh well solution containing 2 mM MBP and incubation for approximately 60 s, the crystals were transferred again to a cryoprotectant well solution containing 2 mM MBP and 30% (v/v) glycerol and flash-frozen in liquid nitrogen.

X-ray Data Collection. Crystals were irradiated at the Advanced Photon Source at Argonne National Laboratory (Argonne, IL), using the 23-IDD beamline administered by GM/CA-CAT. The data were scaled in I_{222}, the same space group previously reported for wild-type BFDC in the absence of inhibitor. The HKL 2000 software package and the CCP4 suite of programs were used for data reduction and processing (*28, 29*). A search model for molecular replacement was obtained from the crystal structure of Hasson et al. (PDB ID 1BFD) (*27*). As was the case for BFDC itself, the asymmetric unit of the BFDC-MBP complex was determined to contain a single monomer. Subsequent refinement of the model was carried out as described below, and crystallization and refinement statistics are given in Table 1.

Table 1: Data, Model, and Crystallographic Statistics for BFDC-MBP Structure (3FSJ)

data set	BFDC with MBP
beamline	APS, GM/CA-CAT, 23-IDD
wavelength (Å)	1.0332
space group	I_{222}
unit cell (Å)	$a = 81.4$, $b = 95.4$, $c = 137.1$
resolution limits (Å)	50.0−1.37 (1.41−1.37)
total reflections	820130
unique reflections	109983
completeness (%) (last shell)	98.3 (96.4)
redundancy (last shell)	7.5 (7.3)
$I/\sigma(I)$ (last shell)	41.7 (7.9)
R_{merge} (last shell)	0.04 (0.27)
unit cell contents	
molecules/ASU	1
solvent content (%)	48.2
refinement statistics	
resolution range (Å)	50.0−1.37
R_{work} (%)	14.9
R_{free} (%)	16.6
no. of residues	522
no. of waters	487
B factors (Å^2)	
average from Wilson plot	17.7
average for ThDP atoms	12.8
average for MBP atoms	27.7
rmsd	
bond lengths (Å)	0.02
bond angles (deg)	2.0
Ramachandran analysis	
most favored (%)	98.5
allowed (%)	100

Structural Refinement. The initial model resulting from molecular replacement was refined using Refmac5 (*30*). Placement of water molecules into difference density peaks with an intensity greater than 3σ was carried out by the water-picking algorithm in Coot 0.4.1 (*31*). Individual water molecules were checked for spherical electron density and the existence of at least one appropriately positioned hydrogen-bonding partner. Water molecules in the vicinity of the active site were removed. After refinement with a model including all nonactive site water molecules, placement of the ThDP cofactor into the positive difference density proceeded, again using Coot. The model containing nonactive site water molecules, the polypeptide chain, and the ThDP cofactor was refined to generate an omit map for the MBP. Coordinate files and appropriate restraints for the unreacted MBP, as well as both enantiomers of the likely adduct, were generated using the Sketcher program of the CCP4 suite and the PRODRG server (*29, 33*). Given the fairly high spatial resolution of the structure, the best-fitting species was unequivocally the MBP-ThDP adduct (see Discussion). In order to independently cross-validate the model, the structure was independently solved using the automated molecular replacement routine of Phenix1.3b (*32*), starting with the model from 1BFD. The simulated annealing omit map generated in Phenix was in excellent agreement with that

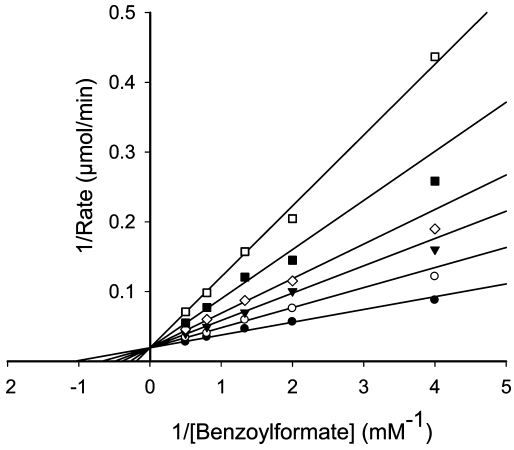

FIGURE 1: Concentration dependence of inhibition of BFDC by MBP. The MBP concentration was held at (●) 0, (○) 0.25, (▼) 0.5, (◇) 0.75, (■) 1.25, and (□) 2 mM while the benzoylformate concentration was varied between 0.3−3 × K_m.

produced from CCP4. The final structural solution was subjected to validation using SFCheck and ProCheck 3.4.4, deposited in the Protein Data Bank, and assigned a PDB ID of 3FSJ (*34, 35*).

RESULTS

Reaction of BFDC with Methyl Benzoylphosphonate and Methyl Acetylphosphonate. (A) Methyl Benzoylphosphonate Is a Competitive Inhibitor of BFDC. The steady-state kinetic data in Figure 1 show that MBP, a close structural and electrostatic analogue of the true substrate benzoylformate, is a competitive inhibitor of BFDC. The data provided a K_i value for MBP of 0.38 ± 0.04 mM. By comparison, the K_m value for benzoylformate was found to be 0.76 ± 0.09 mM.

(B) Circular Dichroism Evidence of the Formation of the 1′, 4′-Iminopyrimidine Tautomeric Form of C2α-Phosphonomandelyl-ThDP on BFDC. Incremental addition of MBP to BFDC produced a positive CD band with λ_{max} at 299 nm in the difference CD spectra of BFDC, corresponding to the 1′,4′-iminopyrimidine tautomer of C2α-phosphonomandelyl-ThDP (PMThDP) (Figure 2A). The amplitude of this band increased with increasing concentration of MBP and displayed saturation with a $K_{d,MBP}$ = 0.113 mM (average from three independent experiments; see Figure 2B for an example) as compared with $K_{i,MBP}$ = 0.38 ± 0.04 mM obtained from kinetics. The CD band at 299 nm was not detected on BFDC after the overnight dialysis, indicating that the formation of 1′,4′-imino-PMThDP is reversible. Next, stopped-flow CD was used to determine the rate of formation of 1′,4′-imino-PMThDP on BFDC (Scheme 1a and Figure 2C). A positive CD band at 305 nm developed with time, which followed an exponential growth to maximum with a rate constant of 2.08 s^{-1}.

(C) Formation of the 1′,4′-Iminopyrimidine Tautomeric Form of Phosphonolactyl-ThDP on BFDC. Methyl acetylphosphonate (MAP) is similar to MBP characterized above, but with a methyl group replacing the phenyl ring in MBP. A comparison of the behavior of MAP and MBP would throw light on the substrate specificity of BFDC. A CD titration of BFDC with MAP revealed the development of the same positive CD band at 299 nm (Figure 3A), a characteristic of 1′,4′-iminophosphonolactyl-ThDP (PLThDP), the covalent

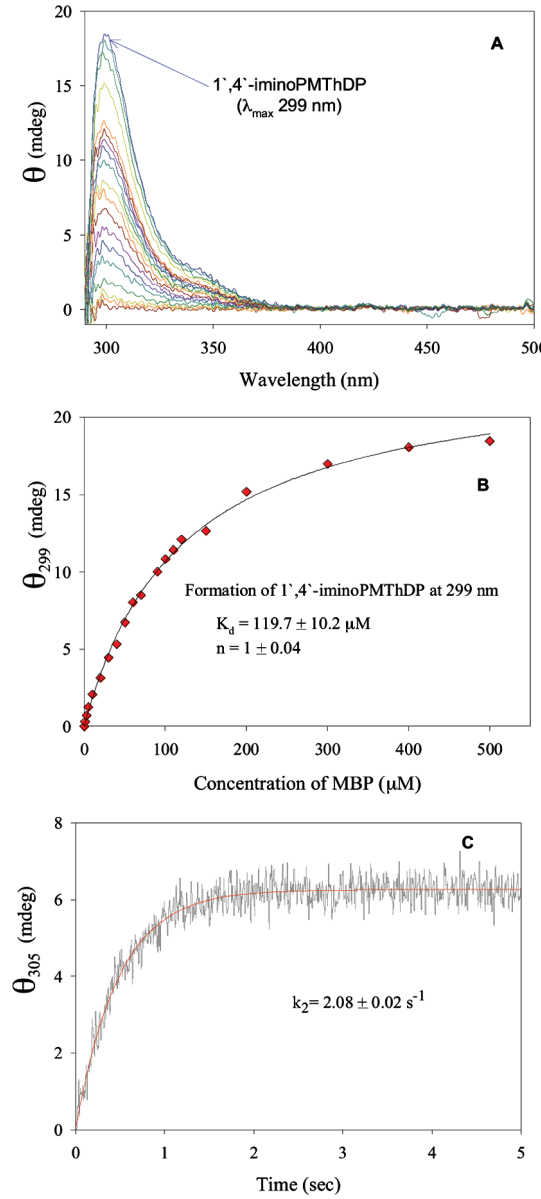

FIGURE 2: Circular dichroism studies of the binding of MBP to BFDC. (A) Difference CD spectra showing formation of 1′,4′-imino-PMThDP on BFDC. Conditions are described in Materials and Methods. (B) Changes in ellipticity at 299 nm with increasing concentration of MBP in panel A. (C) Rate of 1′,4′-imino-PMThDP formation monitored on stopped-flow CD when BFDC (66.4 μM active site concentration) in 50 mM KH_2PO_4 (pH 6.0) was mixed with an equal volume of 4 mM MBP in the same buffer at 30 °C. Reaction was monitored for 5 s at 305 nm with a path length of 1 cm and slit width of 2 nm. A total of 5000 data points were collected at 5 ms intervals.

adduct between MAP and ThDP, already reported on yeast pyruvate decarboxylase (YPDC) and the E1 component of *Escherichia coli* pyruvate dehydrogenase (*36*−*40*). The K_d for MAP was 5.49 mM (Figure 3A, inset), 55 times larger than that for MBP. Overnight dialysis again eliminated the CD band at 299 nm (Figure 3B), indicating that the formation of the PLThDP is reversible.

(D) Evidence for Formation of PMThDP on BFDC by Mass Spectrometry. The formation of the adduct between ThDP and MBP on BFDC was confirmed by mass spectral analysis. The BFDC was titrated by MBP, and formation of the positive CD band at 299 nm was monitored. Once the titration was completed, 12.5% TCA was added to precipitate

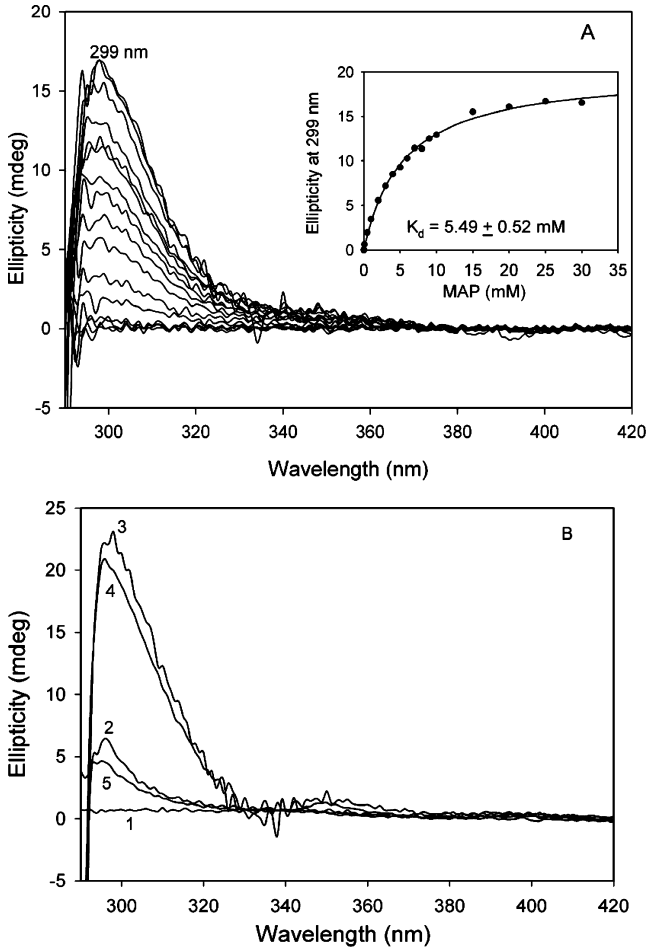

FIGURE 3: Circular dichroism titration of BFDC with MAP. (A) Difference spectra of BFDC (1.7 mg/mL, concentration of active centers = 30.2 μM) on addition of 1−30 mM MAP. The conditions of the experiments are described in Materials and Methods. Inset: Dependence of the ellipticity at 299 nm on concentration of MAP. (B) The reversibility of 1′, 4′-iminophosphonolactyl-ThDP formation on BFDC: 1, baseline recorded with 10 mM KH_2PO_4 (pH 6.0); 2, BFDC (1.70 mg/mL) in the presence of 2.50 mM $MgCl_2$ and 0.50 mM ThDP; 3, BFDC as in line 2 with 30 mM MAP; 4, as in line 3 after overnight incubation at 4 °C; 5, as in line 4 after 3 h of dialysis against 2 L of 20 mM KH_2PO_4 (pH 6.0).

the protein. The supernatant was analyzed for products by FTICR mass spectrometry. The species with mass of 625.0628 Da (M^+) and mass of 626.0661 $(M + 1)^+$ were identified as PMThDP, confirming its formation on BFDC (Figure 4).

(E) Structure of the Covalent Adduct. The structural consequence of addition of ThDP ylide to MBP is the formation of a tetrahedral center at the 2′ carbon (Scheme 2). The electron density after refinement of the structural model, including the cofactor, clearly shows tetrahedral positive difference density above the plane of the cofactor, along with a ring of density at an angle to the plane of the thiazolium ring (Figure 5). This electron density is relatively well fit by a tetrahedral adduct of ThDP and MBP but not by the planar sp^2-hybridized unbound MBP. In the initial refinement stages, the adduct C2α-phosphonomandelyl-ThDP (PMThDP) was modeled independently of the cofactor. Given the covalent adduct PMThDP that is formed, subsequent rounds of refinement involved fitting PMThDP. The best fit is obtained when the C−C distance between C2 and C2α is somewhat longer than a typical C−C bond. Thus, it is likely that the observed electron density represents a mixture of species in the active site. Some positive difference density is observable near the phenyl ring and phosphonate group of bound MBP, again suggesting multiple conformations. This C−C distance between C2 and C2α is in contrast to the observed electron density for BAL with MBP, where the same distance was observed to be 1.5 Å (*22*). This difference may result from differences in experimental conditions. In any case, it is clear that the observed electron density is best fit by the covalent adduct between ThDP and MBP.

DISCUSSION

Methyl Benzoylphosphonate Forms a Stable Predecarboxylation Intermediate Analogue. The compound MBP behaved as a mechanism-based, competitive, reversible inhibitor of BFDC ($K_i = 0.38 \pm 0.04$ μM) (Figure 1). The spectroscopic signal for the covalent adduct formed was characteristic of C2α-phosphonomandelyl-ThDP, a stable MThDP analogue. Earlier, the use of MAP with ThDP-dependent enzymes YPDC and *E. coli* PDHc E1 enabled the observation of a positive CD band in the 300−305 nm region (*41, 42*). Model studies showed (*37, 43*) that formation of the 1′,4′-iminopyrimidine tautomer accounts for this electronic transition (*37*−*40, 42, 44*−*46*). Accordingly, the band with an absorption maximum at 299 nm (Figure 2A) was attributed to the 1′,4′-imino-PLThDP. Addition of both MBP and MAP produced the same positive band (λ_{max} 299 nm; Figures 2 and 3). A rate constant of 2.08 s^{-1} was obtained by stopped-flow CD of BFDC with MBP for formation of the band and, by extension, for covalent bond formation (Figure 2C).

Involvement of ThDP 4′-Aminopyrimidinium Ring. The role of the 4′-aminopyrimidine ring in the catalytic cycle of ThDP-dependent enzymes has been a central point of interest for a long time (*37*−*40, 42*−*45, 47*−*51*). The MBP-ThDP adduct observed here (PMThDP) is a stable analogue of MThDP, so the observations above likely apply to reaction with the native substrate. The formation of the 1′,4′-imino tautomer of MThDP could be explained by the mechanism shown in Scheme 2. The 4′-aminopyrimidine ring undergoes protonation at N1′ by a conserved glutamate, forming 4′-aminopyrimidinium-ThDP, which loses a proton to form 1′,4′-imino-ThDP (IP form of the cofactor, $\lambda_{max} = 299$ nm). The imino nitrogen then abstracts the proton from C2−H of thiazolium, producing the ylide and the 4′-aminopyrimidinium-ThDP (APH^+). The ylide carries out a nucleophilic attack on the incoming α-keto acid at its carbonyl carbon, producing the C2α-oxyanion which picks up the proton to form the 1′,4′-imino-MThDP. We have suggested that the tetrahedral ThDP-bound intermediates on all ThDP-dependent enzymes exist in their 1′,4′-imino tautomeric forms (*38*).

The spectroscopic evidence points clearly to the existence of the IP form of the cofactor. Indeed, recently evidence was provided for formation of such a PMThDP adduct on BAL (*21, 22*).

Role of Active Site Residues in BFDC-Catalyzed Decarboxylation. Several hypotheses have been put forward to explain how BFDC accelerates the rate of decomposition over the uncatalyzed, spontaneous decarboxylation of the C2α-mandelylthiamin diphosphate intermediate (*52*). The

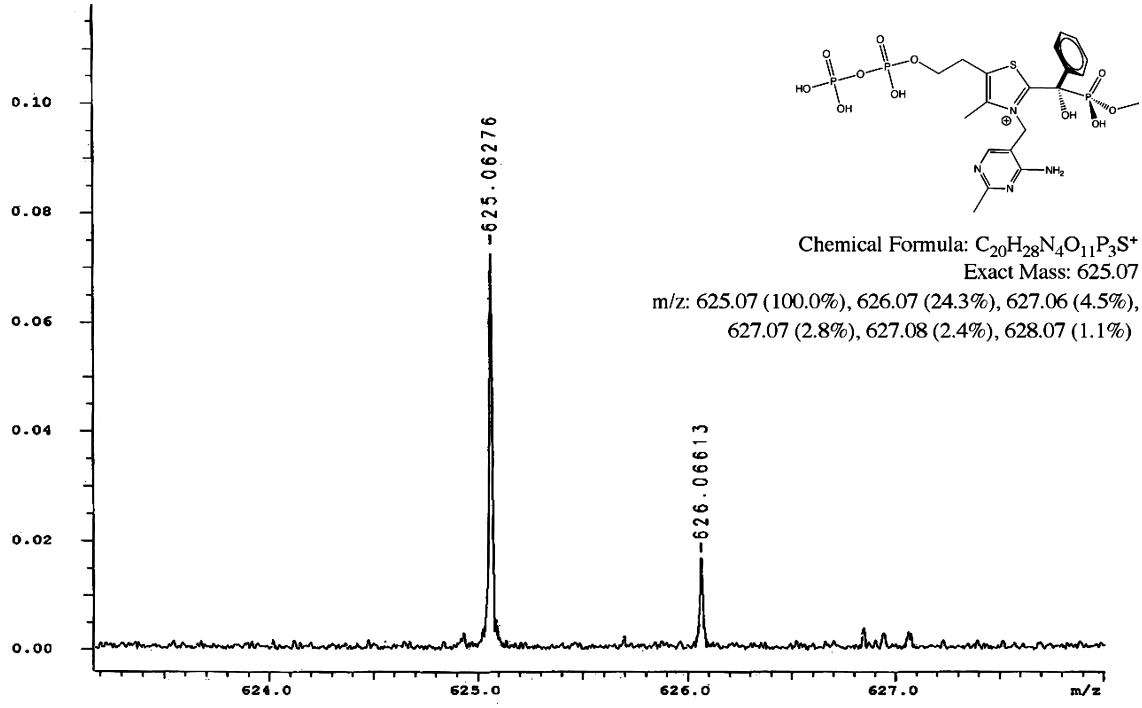

FIGURE 4: Evidence for the formation of a covalent adduct between the cofactor ThDP and the mechanism-based inhibitor MBP by FTICR mass spectrometry. Cofactor adduct was identified from reaction mixture subsequent to TCA precipitation of protein.

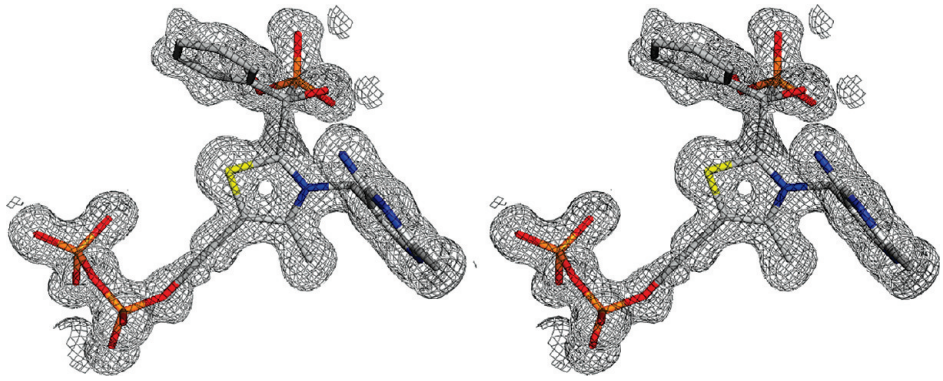

FIGURE 5: Electron density maps (gray mesh) for the BFDC-bound MBP-ThDP adduct, demonstrating the occupancy of the inhibitor phenyl ring and confirming the presence of electron density resulting from the newly formed bond. The indicated electron density results from a simulated annealing refined $2F_o - F_c$ omit map contoured to 0.9σ (PDB ID 3FSJ).

current thinking postulates that the primary source of this acceleration is not maintenance of the adduct in a hydrophobic environment but rather positioning of acidic residues to protonate the carbanion that forms upon decarboxylation (*53*). These residues were proposed to be His70 and His281, on the grounds of proximity and that replacement of the imidazole ring of His70 and His281 can lead to significant reduction in k_{cat} (*54*). The present crystal structure of the MBP adduct shows that the closest heavy-atom approach between the C2α anion and atoms of either histidine is >5 Å (Figure 6). In addition, the catalyzed rate is a million-fold greater than the uncatalyzed rate, where replacement of His281 by alanine is accompanied by a roughly 200-fold rate reduction (*54*). Recent saturation mutagenesis experiments have thoroughly examined the side chain tolerance of His70 and His281, as well as Ser26 (*26*). Surprisingly, these protic active site residues can be replaced by hydrophobic amino acids with relatively modest reduction in catalytic efficiency (on the order of 10-fold), as measured by k_{cat}/K_m. Together with these mutational data, the current structure leads us to propose a potential role for promotion of decarboxylation by stabilization of a particular substrate geometry rather than proton transfer. Interaction of the substrate carboxylate with His281, for example, could position the carboxylate over the thiazolium ring, whereas interaction with Ser26 would place the plane of the carboxylate perpendicular to the thiazolium−C2α bond and out of range of interaction with the thiazolium π system. These conformations may promote decarboxylation to a different extent or via a slightly different reaction coordinate. Future examination of the relative energetics of these conformations may provide insight into the role of polar active site residues in positioning benzoylformate for decarboxylation in the BFDC active site. The replacement of these residues with large hydrophobic sidechains, such as leucine or phenylalanine, may influence the localization of negative charge onto the two carboxylate oxygens, also an issue that lends itself to theoretical study.

Comparing BFDC-MBP and BAL-MBP Structures. Benzaldehyde lyase is a ThDP-dependent enzyme that carries

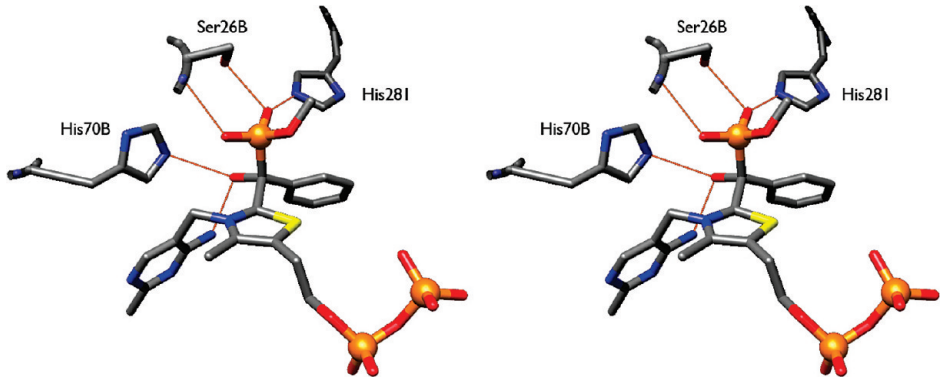

FIGURE 6: Stereoview of binding geometry of the MBP-ThDP adduct of benzoylformate decarboxylase (BFDC), showing likely hydrogen bonds between enzyme and adduct.

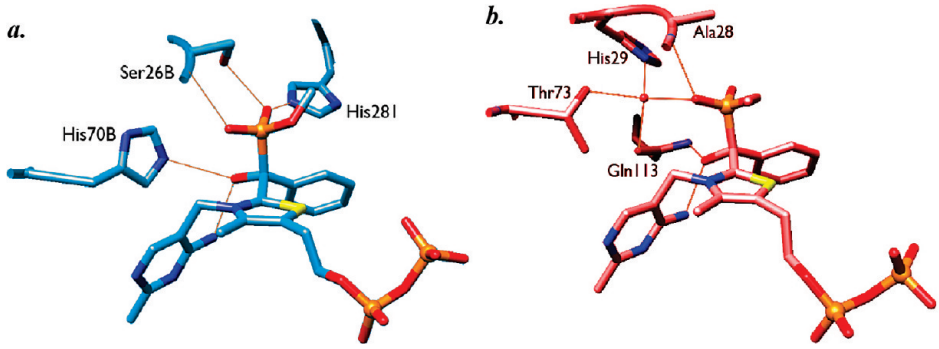

FIGURE 7: Comparison of the inhibitor MBP bound in the active sites of benzoylformate decarboxylase (BFDC, a) and benzaldehyde lyase (BAL, b).

Scheme 3: Schematic of Mechanism of BFDC-Catalyzed HPP Formation from Benzaldehyde and Acetaldehyde (a) and Relationship (b) of ThDP-MBP Complex to Penultimate Intermediate (Boxed at Right)

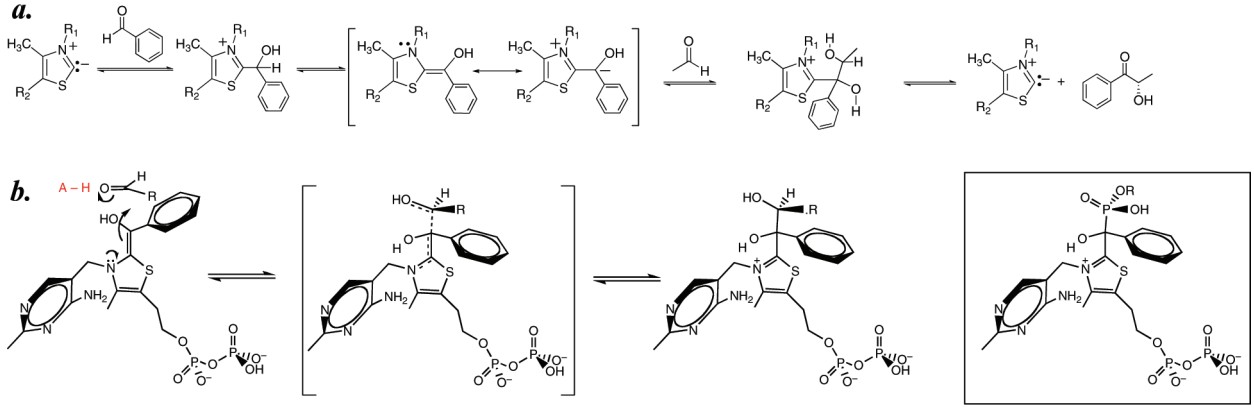

out the reversible conversion of (*R*)-benzoin to benzaldehyde (*21, 55*−*57*) (Scheme 1). Although BFDC and BAL are homologous (27% sequence identity), few active site residues are conserved, and BFDC is essentially inactive toward benzoin (*21, 56*). Likewise, BAL has very little decarboxylase activity, although its A28S variant does exhibit significant BFDC activity (*56*). Nonetheless, the two enzymes carry out very similar carboligation reactions in that both condense 2 equiv of benzaldehyde to give (*R*)-benzoin with very high enantioselectivity (>98% ee). However, one intriguing distinction between BFDC and BAL is that they give products with the opposite stereochemistry in a mixed acyloin condensation reaction. For example, BFDC condenses benzaldehyde and acetaldehyde to produce 2-(*S*)-hydroxypropiophenone (HPP) with >90% ee, whereas BAL generates the *R*-enantiomer with >99% ee (*58*).

Alignment of the two structures shows the differences in active site residues directly contacting the MBP (Figure 7). A notable distinction is the orientation of the phosphonate hydrogen-bonding network in the BFDC active site relative to that of BAL (*22*). Where BFDC has the possibility for orienting the substrate toward Ser26 or toward His281, BAL supports only orientation toward Ala28 (the structural homologue of Ser26) and the ordered water positioned there.

Active Site Residues Important to Formation of 2-HPP from Acetaldehyde and Benzaldehyde. The complex of BFDC and BAL with MBP mimics the result of addition of the donor benzaldehyde to acceptor acetaldehyde, the penultimate and stereogenic step of the carboligation reaction (Scheme 3). Taking the three phosphonate oxygens to represent three possible oxygen binding sites of the single oxygen of the reaction intermediate, considering both

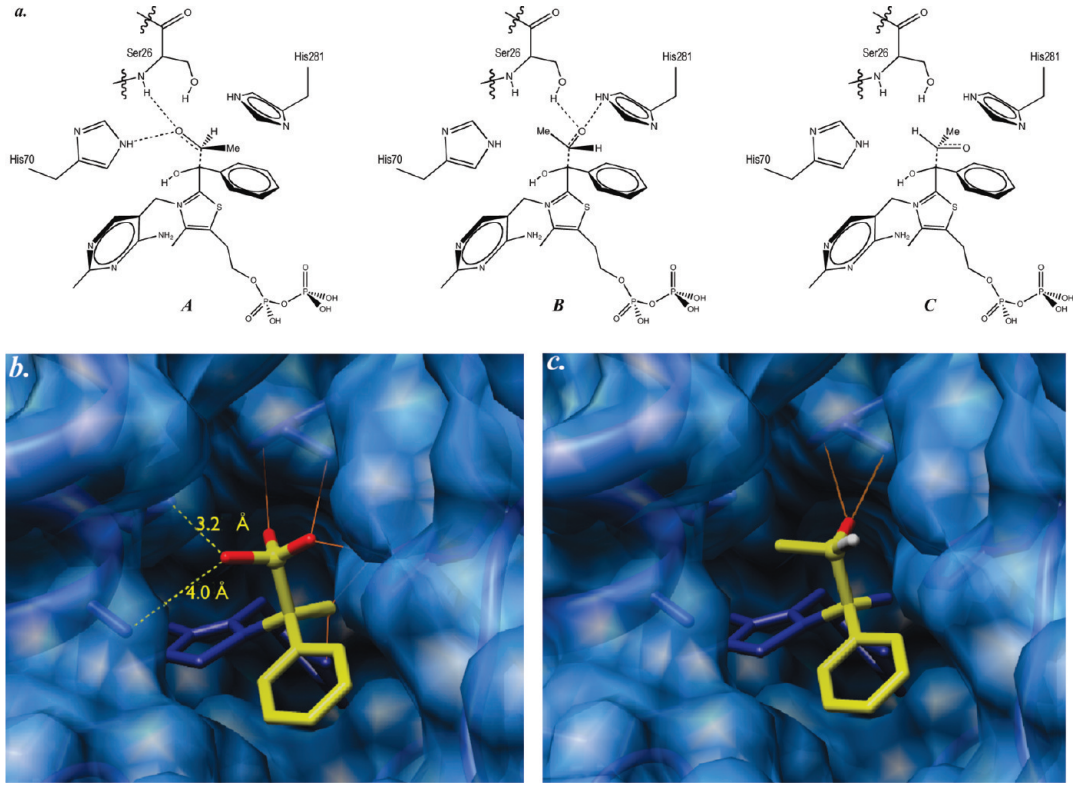

FIGURE 8: Possible conformations for ThDP-bound HPP intermediate, based on the observed (*S*) stereochemistry of the 2-HPP product. (a) Schematic of available conformations for HPP intermediate. (b) Active site of BFDC with MBP. Likely hydrogen bonds are indicated in orange. Heavy atom distances to nearest atoms of residues making up the methyl binding pocket are shown in yellow. (c) Active site of BFDC with predicted geometry of ThDP-bound HPP intermediate model.

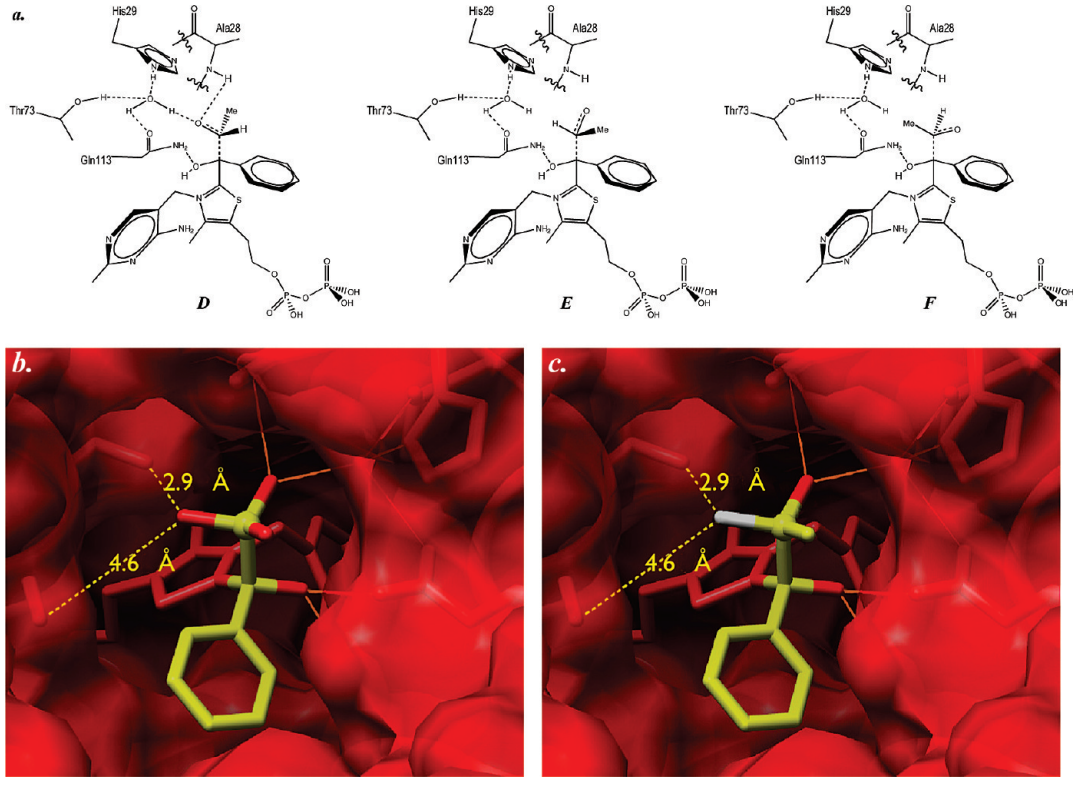

FIGURE 9: Analysis of intermediate binding to the BAL active site. (a) Predicted geometry of ThDP-bound HPP intermediate for BAL, based on observed (*R*) stereochemistry of 2-HPP product and favorable interaction with His29-positioned water. (b) View of the BAL active site with MBP bound. Note that schematic and surface views are rotated ~90° relative to each other. (c) View of BAL with predicted ThDP-bound HPP intermediate.

configurations for each conformation leads to six possibilities. Disregarding those that would give rise to 2-(*R*)-HPP (which is not observed) leaves three possible conformations to consider (Figure 8a). In addition to the likely hydrogen bonds

indicated above, Figure 8b shows potential stabilizing hydrophobic interactions for a substrate methyl group (yellow lines showing heavy-atom distances to nearest atom of the relevant hydrophobic residue) (*9, 10*). Stabilization of the carbinol oxygen by two side chains, a proper fit into the small hydrophobic pocket of the methyl group, and the presence of His281 as a potential proton donor/acceptor support the likelihood of a conformation like that of panel B. Note that the MBP-ThDP adduct lacks the methyl group to nestle into the methyl binding pocket. We would expect the best fit to result from a ~15° clockwise rotation around the C2α−P bond (viewed from above). This rotation brings the hydroxyl group into a position that preserves the interaction with Ser26 but loses that with His281 (Figure 8c). His281 is not a necessary residue for catalysis of 2-HPP formation. Indeed, mutation to alanine results in an approximately 125-fold increase in catalytic rate (*15*), perhaps because the removal of the imidazole side chain favors a more productive binding mode wherein the methyl binding pocket and Ser26 dominate substrate positioning.

Carboligation Reactions Catalyzed by BAL. A similar analysis may be undertaken for condensation of benzaldehyde with acetaldehyde catalyzed by BAL, which gives the opposite enantiomer of HPP to that given by BFDC (*58*) (Figure 9). Of the three pro-*R* conformations available to BAL, D would seem to be preferred, as it is the only one of the three in which a hydrogen-bonding interaction is available to the 2-hydroxyl group of the ThDP-bound HPP intermediate. This conformation also has the effect of positioning the methyl group of acetaldehyde in the more open portion of the active site cleft. The methyl binding pocket observed in BFDC is occluded in BAL by the γ-methyl group of Thr481, which perhaps sets up a steric clash that leads to preferential positioning of the aldehydic proton in this small pocket (*9, 10*). This explanation leads naturally to the prediction that the BAL T481S mutant may well produce 2-(*S*)-HPP, a prediction which is currently under investigation.

Explanation for Observed Stereochemistry of BFDC and BAL Products. This analysis also serves to show why both enzymes produce (*R*)-benzoin. In the case of BAL, both the methyl group of acetaldehyde and the phenyl of benzaldehyde are too bulky to fit in the active site. So, BAL produces (*R*)-benzoin for the same reason it produces 2-(*R*)-HPP. In the case of BFDC, we argued that binding the methyl group of acetaldehyde in the methyl binding pocket gave rise to the *S*-product. This pocket, however, fails to accommodate the phenyl ring of benzaldehyde. Now, when the acceptor benzaldehyde binds, it positions its aldehydic proton to enter the methyl binding pocket, the carbonyl oxygen to interact with Ser26, and the phenyl group to occupy the mouth of the active site cleft (Figure 8). This is a similar binding mode to that proposed for BAL and correspondingly generates the *R*-product.

The same explanation holds for recent studies showing that BFDC-catalyzed condensation of benzaldehyde with propanal overwhelmingly produces the *R*-product, while a point mutant of the enzyme gives the *S*-product (*9*). Increasing the space available in the active site by converting Leu461 to Ala permits the substrate to orient itself in such a way that the propane side chain can be tucked into the created space, generating the *S*-product.

CONCLUSION

The work presented here seeks to characterize formation of the predecarboxyation covalent adduct between the inhibitor MBP and the ThDP cofactor of the enzyme BFDC. MBP was shown to be a mechanism-based inhibitor of BFDC, by determining the parameters of its inhibition of the enzyme and also by mass spectrometric analysis of the cofactor adduct isolated from the reaction mixture. In addition, the rate of formation of the covalent adduct was followed in real time by stopped-flow CD, and the results were interpreted in light of the increasing understanding of ThDP activation in a variety of ThDP-dependent enzymes. Finally, the crystal structure of the covalent adduct was solved. The BFDC-MBP adduct is of particular interest, since an analysis of this protein-inhibitor complex may shed light on the detailed mechanism of BFDC. This enzyme has been employed as a biocatalyst for the asymmetric production of 2-hydroxy ketones, as has the related enzyme BAL. The two enzymes catalyze the production of opposite enantiomers for the condensation of benzaldehyde with acetaldehyde. The source of this stereospecificity is examined in light of structures available for the covalent complex of both enzymes with the same MBP inhibitor. Altogether, this work provides a detailed analysis of the first step in the mechanism of benzoylformate decarboxylation and its functional consequences.

REFERENCES

1. Bugg, T. D. H. (2001) The development of mechanistic enzymology in the 20th century. *Nat. Prod. Rep. 18*, 465–493.
2. Kraut, D. A., Carroll, K. S., and Herschlag, D. (2003) Challenges in enzyme mechanism and energetics. *Annu. Rev. Biochem. 72*, 517–571.
3. Garcia-Viloca, M., Gao, J., Karplus, M., and Truhlar, D. G. (2004) How enzymes work: Analysis by modern rate theory and computer simulations. *Science 303*, 186–195.
4. Zhang, X. Y., and Houk, K. N. (2005) Why enzymes are proficient catalysts: Beyond the Pauling paradigm. *Acc. Chem. Res. 38*, 379–385.
5. Naismith, J. H. (2006) Inferring the chemical mechanism from structures of enzymes. *Chem. Soc. Rev. 35*, 763–770.
6. Ringe, D., and Petsko, G. A. (2008) How enzymes work. *Science 320*, 1428–1429.
7. Kennedy, S. I., and Fewson, C. A. (1968) Enzymes of the mandelate pathway in *Bacterium N.C.I.B. 8250*. *Biochem. J. 107*, 497–506.
8. Hegeman, G. D. (1970) Benzoylformate decarboxylase (*Pseudomonas putida*). *Methods Enzymol. 17A*, 674–678.
9. Gocke, D., Walter, L., Gauchenova, E., Kolter, G., Knoll, M., Berthold, C. L., Schneider, G., Pleiss, J., Muller, M., and Pohl, M. (2008) Rational protein design of ThDP-dependent enzymes-engineering stereoselectivity. *ChemBioChem 9*, 406–412.
10. Knoll, M., Muller, M., Pleiss, J., and Pohl, M. (2006) Factors mediating activity, selectivity, and substrate specificity for the thiamin diphosphate-dependent enzymes benzaldehyde lyase and benzoylformate decarboxylase. *ChemBioChem 7*, 1928–1934.
11. Siegert, P., McLeish, M. J., Baumann, M., Iding, H., Kneen, M. M., Kenyon, G. L., and Pohl, M. (2005) Exchanging the substrate specificities of pyruvate decarboxylase from *Zymomonas mobilis* and benzoylformate decarboxylase from *Pseudomonas putida*. *Protein Eng. Des. Sel. 18*, 345–357.
12. Yep, A., Kenyon, G. L., and McLeish, M. J. (2006) Determinants of substrate specificity in KdcA, a thiamin diphosphate-dependent decarboxylase. *Bioorg. Chem. 34*, 325–336.
13. Demir, A. S., Dunnwald, T., Iding, H., Pohl, M., and Muller, M. (1999) Asymmetric benzoin reaction catalyzed by benzoylformate decarboxylase. *Tetrahedron: Asymmetry 10*, 4769–4774.
14. Iding, H., Dunnwald, T., Greiner, L., Liese, A., Muller, M., Siegert, P., Grotzinger, J., Demir, A. S., and Pohl, M. (2000) Benzoylfor-

mate decarboxylase from *Pseudomonas putida* as stable catalyst for the synthesis of chiral 2-hydroxy ketones. *Chem. Eur. J. 6*, 1483–1495.
15. Dunkelmann, P., Kolter-Jung, D., Nitsche, A., Demir, A. S., Siegert, P., Lingen, B., Baumann, M., Pohl, M., and Muller, M. (2002) Development of a donor-acceptor concept for enzymatic cross-coupling reactions of aldehydes: the first asymmetric cross-benzoin condensation. *J. Am. Chem. Soc. 124*, 12084–12085.
16. Pohl, M., Sprenger, G. A., and Muller, M. (2004) A new perspective on thiamine catalysis. *Curr. Opin. Biotechnol. 15*, 335–342.
17. O'Brien, T. A., Kluger, R., Pike, D. C., and Gennis, R. B. (1980) Phosphonate analogues of pyruvate. Probes of substrate binding to pyruvate oxidase and other thiamin pyrophosphate-dependent decarboxylases. *Biochim. Biophys. Acta 613*, 10–17.
18. Arjunan, P., Sax, M., Brunskill, A., Chandrasekhar, K., Nemeria, N., Zhang, S., Jordan, F., and Furey, W. (2006) A thiamin-bound, pre-decarboxylation reaction intermediate analogue in the pyruvate dehydrogenase E1 subunit induces large scale disorder-to-order transformations in the enzyme and reveals novel structural features in the covalently bound adduct. *J. Biol. Chem. 281*, 15296–15303.
19. Seifert, F., Golbik, R., Brauer, J., Lilie, H., Schroder-Tittmann, K., Hinze, E., Korotchkina, L. G., Patel, M. S., and Tittmann, K. (2006) Direct kinetic evidence for half-of-the-sites reactivity in the E1 component of the human pyruvate dehydrogenase multienzyme complex through alternating sites cofactor activation. *Biochemistry 45*, 12775–12785.
20. Wille, G., Meyer, D., Steinmetz, A., Hinze, E., Golbik, R., and Tittmann, K. (2006) The catalytic cycle of a thiamin diphosphate enzyme examined by cryocrystallography. *Nat. Chem. Biol. 2*, 324–328.
21. Chakraborty, S., Nemeria, N., Yep, A., McLeish, M. J., Kenyon, G. L., and Jordan, F. (2008) Mechanism of benzaldehyde lyase studied via thiamin diphosphate-bound intermediates and kinetic isotope effects. *Biochemistry 47*, 3800–3809.
22. Brandt, G. S., Nemeria, N., Chakraborty, S., McLeish, M. J., Yep, A., Kenyon, G. L., Petsko, G. A., Jordan, F., and Ringe, D. (2008) Probing the active center, of benzaldehyde lyase with substitutions and the pseudosubstrate analogue benzoylphosphonic acid methyl ester. *Biochemistry 47*, 7734–7743.
23. Demir, A. S., Sesenoglu, O., Eren, E., Hosrik, B., Pohl, M., Janzen, E., Kolter, D., Feldmann, R., Dunkelmann, P., and Muller, M. (2002) Enantioselective synthesis of alpha-hydroxy ketones via benzaldehyde lyase-catalyzed C-C bond formation reaction. *Adv. Synth. Catal. 344*, 96–103.
24. Demir, A. S., Sesenoglu, O., Dunkelmann, P., and Muller, M. (2003) Benzaldehyde lyase-catalyzed enantioselective carboligation of aromatic aldehydes with mono- and dimethoxy acetaldehyde. *Org. Lett. 5*, 2047–2050.
25. Janzen, E., Muller, M., Kolter-Jung, D., Kneen, M. M., McLeish, M. J., and Pohl, M. (2006) Characterization of benzaldehyde lyase from *Pseudomonas fluorescens*: A versatile enzyme for asymmetric C-C bond formation. *Bioorg. Chem. 34*, 345–361.
26. Yep, A., Kenyon, G. L., and McLeish, M. J. (2008) Saturation mutagenesis of putative catalytic residues of benzoylformate decarboxylase provides a challenge to the accepted mechanism. *Proc. Natl. Acad. Sci. U.S.A. 105*, 5733–5738.
27. Hasson, M. S., Muscate, A., McLeish, M. J., Polovnikova, L. S., Gerlt, J. A., Kenyon, G. L., Petsko, G. A., and Ringe, D. (1998) The crystal structure of benzoylformate decarboxylase at 1.6 Å resolution: diversity of catalytic residues in thiamin diphosphate-dependent enzymes. *Biochemistry 37*, 9918–9930.
28. Bailey, S. (1994) The CCP4 suite—programs for protein crystallography. *Acta Crystallogr. D50*, 760–763.
29. Potterton, E., Briggs, P., Turkenburg, M., and Dodson, E. (2003) A graphical user interface to the CCP4 program suite. *Acta Crystallogr. D59*, 1131–1137.
30. Murshudov, G. N., Vagin, A. A., and Dodson, E. J. (1997) Refinement of macromolecular structures by the maximum-likelihood method. *Acta Crystallogr. D53*, 240–255.
31. Emsley, P., and Cowtan, K. (2004) Coot: model-building tools for molecular graphics. *Acta Crystallogr. D60*, 2126–2132.
32. Adams, P. D., Grosse-Kunstleve, R. W., Hung, L. W., Ioerger, T. R., McCoy, A. J., Moriarty, N. W., Read, R. J., Sacchettini, J. C., Sauter, N. K., and Terwilliger, T. C. (2002) PHENIX: building new software for automated crystallographic structure determination. *Acta Crystallogr. D58*, 1948–1954.
33. Schuttelkopf, A. W., and van Aalten, D. M. F. (2004) PRODRG: a tool for high-throughput crystallography of protein-ligand complexes. *Acta Crystallogr. D60*, 1355–1363.
34. Hooft, R. W., Vriend, G., Sander, C., and Abola, E. E. (1996) Errors in protein structures. *Nature 381*, 272.
35. Laskowski, R. A., Macarthur, M. W., Moss, D. S., and Thornton, J. M. (1993) PROCHECK—a program to check the stereochemical quality of protein structures. *J. Appl. Crystallogr. 26*, 283–291.
36. Jordan, F., Nemeria, N. S., Zhang, S., Yan, Y., Arjunan, P., and Furey, W. (2003) Dual catalytic apparatus of the thiamin diphosphate coenzyme: acid-base via the 1′,4′-iminopyrimidine tautomer along with its electrophilic role. *J. Am. Chem. Soc. 125*, 12732–12738.
37. Jordan, F., Zhang, Z., and Sergienko, E. (2002) Spectroscopic evidence for participation of the 1′,4′-imino tautomer of thiamin diphosphate in catalysis by yeast pyruvate decarboxylase. *Bioorg. Chem. 30*, 188–198.
38. Nemeria, N., Baykal, A., Joseph, E., Zhang, S., Yan, Y., Furey, W., and Jordan, F. (2004) Tetrahedral intermediates in thiamin diphosphate-dependent decarboxylations exist as a 1′,4′-imino tautomeric form of the coenzyme, unlike the michaelis complex or the free coenzyme. *Biochemistry 43*, 6565–6575.
39. Nemeria, N., Chakraborty, S., Baykal, A., Korotchkina, L. G., Patel, M. S., and Jordan, F. (2007) The 1′,4′-iminopyrimidine tautomer of thiamin diphosphate is poised for catalysis in asymmetric active centers on enzymes. *Proc. Natl. Acad. Sci. U.S.A. 104*, 78–82.
40. Nemeria, N., Korotchkina, L., McLeish, M. J., Kenyon, G. L., Patel, M. S., and Jordan, F. (2007) Elucidation of the chemistry of enzyme-bound thiamin diphosphate prior to substrate binding: defining internal equilibria among tautomeric and ionization states. *Biochemistry 46*, 10739–10744.
41. Baburina, I., Dikdan, G., Guo, F., Tous, G. I., Root, B., and Jordan, F. (1998) Reactivity at the substrate activation site of yeast pyruvate decarboxylase: inhibition by distortion of domain interactions. *Biochemistry 37*, 1245–1255.
42. Nemeria, N., Tittmann, K., Joseph, E., Zhou, L., Vazquez-Coll, M. B., Arjunan, P., Hubner, G., Furey, W., and Jordan, F. (2005) Glutamate 636 of the *Escherichia coli* pyruvate dehydrogenase-E1 participates in active center communication and behaves as an engineered acetolactate synthase with unusual stereoselectivity. *J. Biol. Chem. 280*, 21473–21482.
43. Baykal, A. T., Kakalis, L., and Jordan, F. (2006) Electronic and nuclear magnetic resonance spectroscopic features of the 1′,4′-iminopyrimidine tautomeric form of thiamin diphosphate, a novel intermediate on enzymes requiring this coenzyme. *Biochemistry 45*, 7522–7528.
44. Baykal, A., Chakraborty, S., Dodoo, A., and Jordan, F. (2006) Synthesis with good enantiomeric excess of both enantiomers of alpha-ketols and acetolactates by two thiamin diphosphate-dependent decarboxylases. *Bioorg. Chem. 34*, 380–393.
45. Jordan, F. (2003) Current mechanistic understanding of thiamin diphosphate-dependent enzymatic reactions. *Nat. Prod. Rep. 20*, 184–201.
46. Meshalkina, L. E., Kochetov, G. A., Brauer, J., Hubner, G., Tittmann, K., and Golbik, R. (2008) New evidence for cofactor's amino group function in thiamin catalysis by transketolase. *Biochem. Biophys. Res. Commun. 366*, 692–697.
47. Jordan, F., and Mariam, Y. H. (1978) N1′-methylthiaminium diiodide—model study on effect of a coenzyme bound positive charge on reaction-mechanisms requiring thiamin pyrophosphate. *J. Am. Chem. Soc. 100*, 2534–2541.
48. Schellenberger, A. (1998) Sixty years of thiamin diphosphate biochemistry. *Biochim. Biophy. Acta 1385*, 177–186.
49. Candy, J. M., Koga, J., Nixon, P. F., and Duggleby, R. G. (1996) The role of residues glutamate-50 and phenylalanine-496 in *Zymomonas mobilis* pyruvate decarboxylase. *Biochem. J. 315* (Part 3), 745–751.
50. Wikner, C., Meshalkina, L., Nilsson, U., Nikkola, M., Lindqvist, Y., Sundstrom, M., and Schneider, G. (1994) Analysis of an invariant cofactor-protein interaction in thiamin diphosphate-dependent enzymes by site-directed mutagenesis. Glutamic acid 418 in transketolase is essential for catalysis. *J. Biol. Chem. 269*, 32144–32150.
51. Kern, D., Kern, G., Neef, H., Tittmann, K., Killenberg-Jabs, M., Wikner, C., Schneider, G., and Hubner, G. (1997) How thiamine diphosphate is activated in enzymes. *Science 275*, 67–70.
52. Kluger, R., and Tittmann, K. (2008) Thiamin diphosphate catalysis: Enzymic and nonenzymic covalent intermediates. *Chem. Rev. 108*, 1797–1833.

53. Kluger, R., and Yu, D. (2006) Protein-enhanced decarboxylation of the covalent intermediate in benzoylformate decarboxylase—Desolvation or acid catalysis. *Bioorg. Chem. 34*, 337–344.
54. Polovnikova, E. S., McLeish, M. J., Sergienko, E. A., Burgner, J. T., Anderson, N. L., Bera, A. K., Jordan, F., Kenyon, G. L., and Hasson, M. S. (2003) Structural and kinetic analysis of catalysis by a thiamin diphosphate-dependent enzyme, benzoylformate decarboxylase. *Biochemistry 42*, 1820–1830.
55. Gonzalez, B., and Vicuna, R. (1989) Benzaldehyde lyase, a novel thiamine PPi-requiring enzyme, from *Pseudomonas fluorescens* biovar I. *J. Bacteriol. 171*, 2401–2405.
56. Kneen, M. M., Pogozheva, I. D., Kenyon, G. L., and McLeish, M. J. (2005) Exploring the active site of benzaldehyde lyase by modeling and mutagenesis. *Biochim. Biophys. Acta 1753*, 263–271.
57. Mosbacher, T. G., Mueller, M., and Schulz, G. E. (2005) Structure and mechanism of the ThDP-dependent benzaldehyde lyase from *Pseudomonas fluorescens*. *FEBS J. 272*, 6067–6076.
58. Faber, K., and Kroutil, W. (2005) New enzymes for biotransformations. *Curr. Opin. Chem. Biol. 9*, 181–187.

BI801950K